J. Cent. South Univ. (2015) 22: 1132−1140
DOI: 10.1007/s11771-015-2625-4

Springer

Flow of Casson nanofluid with viscous dissipation and convective conditions: A mathematical model

T. HUSSAIN[1], S. A. SHEHZAD[2], A. ALSAEDI[3], T. HAYAT[3, 4], M. RAMZAN[1]

1. Department of Mathematics, Faculty of Computing, Mohammad Ali Jinnah University, Islamabad Campus 44000, Pakistan;
2. Department of Mathematics, Comsats Institute of Information Technology, Sahiwal 57000, Pakistan;
3. Department of Mathematics, Faculty of Science, King Abdulaziz University, P. O. Box 80257, Jeddah 21589, Saudi Arabia;
4. Department of Mathematics, Quaid-i-Azam University, Islamabad 44000, Pakistan

Abstract: The magnetohydrodynamic (MHD) boundary layer flow of Casson fluid in the presence of nanoparticles is investigated. Convective conditions of temperature and nanoparticle concentration are employed in the formulation. The flow is generated due to exponentially stretching surface. The governing boundary layer equations are reduced into the ordinary differential equations. Series solutions are presented to analyze the velocity, temperature and nanoparticle concentration fields. Temperature and nanoparticle concentration fields decrease when the values of Casson parameter enhance. It is found that the Biot numbers arising due to thermal and concentration convective conditions yield an enhancement in the temperature and concentration fields. Further, we observed that both the thermal and nanoparticle concentration boundary layer thicknesses are higher for the larger values of thermophoresis parameter. The effects of Brownian motion parameter on the temperature and nanoparticle concentration are reverse.

Key words: nanoparticles; Casson fluid; concentration convective condition

1 Introduction

Solar power is a quite natural way to produce heat, electricity, water, and etc. In fact, sustainable energy generation is one of the major issues of present society. Solar energy perhaps has a natural solution with the hourly solar flux incident on the Earth’s surface greater than all of the human consumption of energy in a year. The solar is regarded one of best sources of renewable energy with a minimal environmental impact. Hence, much attention is paid to solar power and solar power technologies utilizations. Nanomaterials are introduced as new energy materials because these materials have particles with size as the same as or smaller than the size of de Broglie wave [1]. The use of nanoparticles is now a subject of abundant studies. It is due to their Brownian motion and thermophoresis properties. A new class of heat transfer fluids is known as nanofluids (a base fluid and nanoparticles). The nanoparticles are utilized to enhance the heat transfer performance of the base fluids [2]. The cooling rate requirements cannot be obtained by the ordinary heat transfer fluids because their thermal conductivity is not adequate. Brownian motion of the nanoparticles enhance the thermal conductivity of base fluids. Further, the magnetic nanofluid is a unique material that has properties of both liquid and magnet. The magnetonano-fluid is important for cancer therapy, construction of loud speakers, blood analysis, and etc. Many of physical characteristics of nanofluids can be controlled and adjusted by varying an applied magnetic field. HOSSEINI and GHADER [3] provided a model to analyze the viscosity of nanofluid with temperature and particle volume fraction. KANDASAMY et al [4] investigated the MHD boundary layer flow over a vertical stretching surface in the presence of nanoparticles. Suction/blowing effects are also considered in this work. They obtained the exact solutions for translational symmetry and numerical solutions for scaling symmetry. Mixed convection flow of nanofluid with magnetic field, suction/injection, viscous dissipation and chemical reaction effects were numerically investigated by KAMESWARAN et al [5]. TURKYILMAZOGLU [6] provided closed form solutions for hydromagnetic thermal slip flow of nanofluid over a linearly stretched surface. Entropy generation analysis in MHD flow of nanofluid was discussed by RASHIDI et al [7]. Here, the flow generation is due to the rotation of porous disk. They provided numerical solutions by employing Runge−Kutta fourth order procedure. Forced convection flow of nanofluid over a horizontal plate was examined

Received date: 2014−04−25; **Accepted date:** 2014−08−06
Corresponding author: T. HUSSAIN, PhD, Lecturer; E-mail: zartotariq@yahoo.com

by HATAMI et al [8]. MAKINDE et al [9] discussed the buoyancy-driven stagnation point flow of nanofluid over a convectively heated stretching and shrinking surfaces. HATAMI and GANJI [10] investigated the effect of heat transfer in non-Newtonian nanofluid passing through a porous medium.

Boundary layer flows with combined heat and mass transfer over a stretching or moving surfaces are quite essential in many industrial and metallurgical processes. Such situations occur in the design of chemical processing, damage of crops due to freezing, cooling of drying and papers in textile, food processing, cooling towers, refrigeration and air conditioning, compact heat exchangers, solar power collectors, cooling of an infinite metallic plate in a cooling bath etc. Various researchers analyzed such flow analysis for different fluid models under isothermal heat and mass conditions (see Refs. [11−15]). Recently, the concept of convective heat condition is quite popular amongst the researchers. For example, AZIZ [16] carried out an analysis to discuss the steady laminar flow over a flat plate with convective boundary condition. MAKINDE and AZIZ [17] extended the work of AZIZ [16] by considering the MHD flow through a porous medium with buoyancy force. HAMAD et al [18] analyzed the variable diffusivity fluid combined with heat and mass transfer in the presence of thermal boundary condition. They discussed the solution employied by LIE group method [18]. Three-dimensional boundary layer flow of Jeffery fluid with convective surface condition was discussed by SHEHZAD et al [19]. HAYAT et al [20] presented homotopic solutions of buoyancy driven flow of Maxwell fluid near a stagnation point in the presence of convective condition. Boundary layer flow of nanofluid with thermal convective boundary condition was investigated by MAKINDE and AZIZ [21]. ALSAEDI et al [22] extended the analysis of Ref. [21] by considering stagnation point flow with heat generation/absorption.

The present investigation is focused on analyzing the effects of convective heat and mass conditions. All above mentioned investigations were presented with constant thermal and concentration conditions or by using the thermal convective boundary condition. The literature on concentration convective condition is not available yet. Further, we considered the magnetohydrodynamic (MHD) boundary layer flow of Casson nanofluid [23−25] over an exponentially stretching surface. Solutions for the velocity, temperature and concentration are computed with the help of homotopy analysis method (HAM) [26−30]. The discussion to plots is given.

2 Problems development

We examine magnetohydrodynamic (MHD) steady flow of Casson nanofluid over an exponentially stretching sheet. The fluid is taken to be incompressible. We assume that the surface of sheet is heated by a hot fluid with temperature T_{f} and concentration C_{f} that give heat and mass transfer coefficients h_1 and h_2. Magnetic field of strength B_0 is applied normally to the flow. The magnetic Reynolds number is chosen to be small. The induced magnetic field is smaller in comparison with the applied magnetic field and thus neglected. The steady MHD boundary layer equations of Casson nanofluid are [21−23]:

$$\frac{\partial u}{\partial x}+\frac{\partial v}{\partial y}=0 \tag{1}$$

$$u\frac{\partial u}{\partial x}+v\frac{\partial u}{\partial y}=\left(1+\frac{1}{\beta}\right)\frac{\partial^2 u}{\partial y^2}-\frac{\sigma B_0^2}{\rho_{\mathrm{f}}}u \tag{2}$$

$$u\frac{\partial T}{\partial x}+v\frac{\partial T}{\partial y}=\alpha\frac{\partial^2 T}{\partial y^2}+\tau\left(D_{\mathrm{B}}\frac{\partial C}{\partial y}\frac{\partial T}{\partial y}+\frac{D_{\mathrm{T}}}{T_\infty}\left(\frac{\partial T}{\partial y}\right)^2\right)+\frac{\nu}{c_p}\left(1+\frac{1}{\beta}\right)\left(\frac{\partial u}{\partial y}\right)^2 \tag{3}$$

$$u\frac{\partial C}{\partial x}+v\frac{\partial C}{\partial y}=D_{\mathrm{B}}\frac{\partial^2 C}{\partial y^2}+\frac{D_{\mathrm{T}}}{T_\infty}\frac{\partial^2 T}{\partial y^2} \tag{4}$$

The boundary conditions for the considered flow analysis are

$$u=u_{\mathrm{w}}(x)=U_0\exp\left(\frac{x}{L}\right),\ v=0,\ -k\frac{\partial T}{\partial y}=h_1(T_{\mathrm{f}}-T),$$

$$-D_{\mathrm{B}}\frac{\partial C}{\partial y}=h_2(C_{\mathrm{f}}-C),\ \text{ at }\ y=0;$$

$$u\to 0,\ v\to 0,\ T\to T_\infty,\ C\to C_\infty,\ \text{ when } y\to\infty \tag{5}$$

where u and v are the velocity components in the x- and y-direction; ν is the kinematic viscosity; β is the Casson parameter; ρ_{f} is the density of fluid; σ is the Steffan−Boltzman constant; α is the thermal diffusivity; $\tau=\dfrac{(\rho c)_{\mathrm{p}}}{(\rho c)_{\mathrm{f}}}$ is the ratio of nanoparticle heat capacity and the base fluid heat capacity; ν is the kinematic viscosity; c_p is the specific heat capacity; D_{B} is the Brownian diffusion coefficient; D_{T} is the thermophoretic diffusion coefficient; k is the thermal conductivity; h_1 and h_2 are the heat and mass transfer coefficients, respectively; T_∞ and C_∞ are the ambient fluid temperature and concentration, respectively.

Equations (2)−(5) can be reduced into the dimensionless form by introducing the following new variables:

$$\eta=y\sqrt{\frac{U_0}{2\nu L}}\exp\left(\frac{x}{2L}\right),\ u=U_0\exp\left(\frac{x}{L}\right)f'(\eta),$$

$$v=-\sqrt{\frac{\nu U_0}{2L}}\exp\left(\frac{x}{2L}\right)(f(\eta)+\eta f'(\eta)),$$

$$A\exp\left(\frac{ax}{2L}\right)\theta(\eta)=\frac{T-T_\infty}{T_\mathrm{f}-T_\infty},\ B\exp\left(\frac{ax}{2L}\right)\phi(\eta)=\frac{C-C_\infty}{C_\mathrm{f}-C_\infty} \tag{6}$$

The equations of linear momentum, energy and concentration in dimensionless form become

$$\left(1+\frac{1}{\beta}\right)f'''+ff''-2f'^2-M^2f'=0 \tag{7}$$

$$\theta''+Prf\theta'+\Pr Nb\theta'\phi'+PrNt\theta'^2+PrEc\left(1+\frac{1}{\beta}\right)f''^2=0 \tag{8}$$

$$\phi''+Lef\phi'+\left(N_t/N_b\right)\theta''=0 \tag{9}$$

$$f=0,\ f'=1,\ \theta'=-Bi_1(1-\theta(0)),\ \phi'=-Bi_2(1-\phi(0));$$
$$\text{at}\ \eta=0,\ f'\to 0,\ \theta\to 0,\ \phi\to 0\ \text{ as}\ \eta\to\infty \tag{10}$$

where $M^2=2\sigma B_0^2L/(\rho_\mathrm{f}U_0\exp(x/L))$ is the magnetic parameter; $Pr=\nu/\alpha$ is the Prandtl number; $Le=\nu/D_\mathrm{B}$ is the Lewis number; $Nb=(\rho c)_\mathrm{p}D_\mathrm{B}(C_\mathrm{f}-C_\infty)/((\rho c)_\mathrm{f}\nu)$ is the Brownian motion parameter; $Nt=(\rho c)_\mathrm{p}D_\mathrm{T}(T_\mathrm{f}-T_\infty)/((\rho c)_\mathrm{f}\nu T_\infty)$ is the thermophoresis parameter; $Bi_1=(h_1/k)\sqrt{\nu/a}$, $Bi_2=(h_2/D_\mathrm{B})\sqrt{\nu/a}$ are the Biot numbers. Equation (1) is satisfied identically.

The skin friction coefficient, the local Nusselt number and the local Sherwood number are

$$C_\mathrm{f}=\frac{\tau_\mathrm{w}}{\rho_\mathrm{f}u_\mathrm{w}^2(x)},\ Nu_x=\frac{xq_\mathrm{w}}{k(T_\mathrm{f}-T_\infty)},$$
$$Sh_x=\frac{xq_\mathrm{m}}{D_\mathrm{B}(C_\mathrm{f}-C_\infty)} \tag{11}$$

where τ_w is the shear stress along the stretching surface; q_w is the surface heat flux; q_m is the surface mass flux. The local skin-friction coefficient, local Nusselt and local Sherwood numbers in dimensionless forms are given below:

$$\sqrt{2Re_x}C_\mathrm{fx}=\left(1+\frac{1}{\beta}\right)f''(0)),\ \sqrt{\frac{2L}{x}}Nu_x/Re_x^{1/2}=-\theta'(0),$$
$$\sqrt{\frac{2L}{x}}Sh_x/Re_x^{1/2}=-\phi'(0) \tag{12}$$

where $Re_x=u_\mathrm{w}(x)L/\nu$ is the local Reynolds number.

3 Homotopy analysis solutions

By choosing a set of base functions: $\{\eta^k\exp(-n\eta),\ k\ge 0, n\ge 0\}$, we can express f, θ and ϕ in the following forms:

$$f_m(\eta)=\sum_{n=0}^{\infty}\sum_{k=0}^{\infty}a_{m,n}^k\eta^k\exp(-n\eta) \tag{13}$$

$$\theta_m(\eta)=\sum_{n=0}^{\infty}\sum_{k=0}^{\infty}b_{m,n}^k\eta^k\exp(-n\eta) \tag{14}$$

$$\phi_m(\eta)=\sum_{n=0}^{\infty}\sum_{k=0}^{\infty}c_{m,n}^k\eta^k\exp(-n\eta) \tag{15}$$

where $a_{m,n}^k$, $b_{m,n}^k$ and $c_{m,n}^k$ are the coefficients. We select the initial guesses and auxiliary linear operators in the following definitions:

$$f_0(\eta)=1-\exp(-\eta),\ \theta_0(\eta)=\frac{Bi_1\exp(-\eta)}{1+Bi_1},$$
$$\phi_0(\eta)=\frac{Bi_2\exp(-\eta)}{1+Bi_2} \tag{16}$$

$$L(f)=f'''-f',\ L(\theta)=\theta''-\theta,\ L(\phi)=\phi''-\phi \tag{17}$$

The above initial guesses and auxiliary linear operators have the properties:

$$L(f)(C_1+C_2e^{\eta}+C_3e^{-\eta})=0,\ L(\theta)(C_4e^{\eta}+C_5e^{-\eta})=0,$$
$$L(\phi)(C_6e^{\eta}+C_7e^{-\eta})=0 \tag{18}$$

where C_i (i=1−7) are the arbitrary constants.

The zeroth order problems are defined as follows:

$$(1-q)L(f)[\bar{f}(\eta;q)-f_0(\eta)]=q\hbar_f\mathbf{N}_f[\bar{f}(\eta;q)] \tag{19}$$

$$(1-q)L(\theta)[\bar{\theta}(\eta;q)-\theta_0(\eta)]=q\hbar_\theta\mathbf{N}_\theta[\bar{f}(\eta;q),\bar{\theta}(\eta,q),$$
$$\bar{\phi}(\eta,q)] \tag{20}$$

$$(1-q)L(\phi)[\bar{\phi}(\eta;q)-\theta_0(\eta)]=q\hbar_\theta\mathbf{N}_\theta[\bar{f}(\eta;q),\bar{\theta}(\eta,q),$$
$$\bar{\phi}(\eta,q)] \tag{21}$$

$$\bar{f}(0;q)=0,\ \bar{f}'(0;q)=1,\ \bar{\theta}'(0,q)=-Bi_1(1-\bar{\theta}(0,q)),$$
$$\bar{\phi}'(0,q)=-Bi_2(1-\bar{\phi}(0,q)),$$
$$\bar{f}'(\infty;q)=0,\ \bar{\theta}(\infty,q)=0,\ \bar{\phi}(\infty,q)=0 \tag{22}$$

$$\mathbf{N}_f[\bar{f}(\eta,q)]=\left(1+\frac{1}{\beta}\right)\frac{\partial^3\bar{f}(\eta,q)}{\partial\eta^3}+\hat{f}(\eta,q)\frac{\partial^2\bar{f}(\eta,q)}{\partial\eta^2}-$$
$$2\left(\frac{\partial\bar{f}(\eta,q)}{\partial\eta}\right)^2-M^2\frac{\partial\bar{f}(\eta,q)}{\partial\eta} \tag{23}$$

$$\mathbf{N}_\theta[\bar{\theta}(\eta,q),\bar{f}(\eta,q),\bar{\phi}(\eta,q)]=\frac{\partial^2\bar{\theta}(\eta,q)}{\partial\eta^2}+$$
$$PrN_\mathrm{b}\frac{\partial\bar{\theta}(\eta,q)}{\partial\eta}\frac{\partial\bar{\phi}(\eta,q)}{\partial\eta}+PrN_\mathrm{t}\left(\frac{\partial\bar{\theta}(\eta,q)}{\partial\eta}\right)^2+$$
$$Pr\,Ec\left(1+\frac{1}{\beta}\right)\left(\frac{\partial^2\bar{f}(\eta,q)}{\partial\eta^2}\right)^2 \tag{24}$$

$$\mathbf{N}_\phi[\bar{\phi}(\eta,q),\bar{f}(\eta,q),\bar{\theta}(\eta,q)]=\frac{\partial^2\bar{\phi}(\eta,q)}{\partial\eta^2}+$$
$$Le\bar{f}(\eta,q)\frac{\partial\bar{\phi}(\eta,q)}{\partial\eta}+(N_\mathrm{t}/N_\mathrm{b})\frac{\partial^2\bar{\theta}(\eta,q)}{\partial\eta^2} \tag{25}$$

In above expressions $\hbar_f$, $\hbar_\theta$ and $\hbar_\phi$ are the non-zero auxiliary parameters; $q \in [0,1]$ is an embedding parameter; $\mathbf{N}_f$, $\mathbf{N}_\theta$ and $\mathbf{N}_\phi$ are the nonlinear operators. Putting q=0 and q=1, one has

$$\bar{f}(\eta;0) = f_0(\eta),\ \bar{\theta}(\eta,0) = \theta_0(\eta),\ \bar{\phi}(\eta,0) = \phi_0(\eta) \text{ and}$$

$$\bar{f}(\eta;1) = f(\eta), \bar{\theta}(\eta,1) = \theta(\eta),\ \bar{\phi}(\eta,1) = \phi(\eta) \tag{26}$$

When we increase the values of q from 0 to 1, $f(\eta,q)$, $\theta(\eta,q)$ and $\phi(\eta,q)$ vary from $f_0(\eta)$, $\theta_0(\eta)$, $\phi_0(\eta)$ to $f(\eta)$, $\theta(\eta)$ and $\phi(\eta)$. Considering Taylor series expansion, one has

$$f(\eta,q) = f_0(\eta) + \sum_{m=1}^{\infty} f_m(\eta) q^m \tag{27}$$

$$\theta(\eta,q) = \theta_0(\eta) + \sum_{m=1}^{\infty} \theta_m(\eta) q^m \tag{28}$$

$$\phi(\eta,q) = \phi_0(\eta) + \sum_{m=1}^{\infty} \phi_m(\eta) q^m \tag{29}$$

$$f_m(\eta) = \frac{1}{m!} \frac{\partial^m f(\eta;q)}{\partial \eta^m}\bigg|_{q=0},\ \theta_m(\eta) = \frac{1}{m!} \frac{\partial^m \theta(\eta;q)}{\partial \eta^m}\bigg|_{q=0},$$

$$\phi_m(\eta) = \frac{1}{m!} \frac{\partial^m \phi(\eta;q)}{\partial \eta^m}\bigg|_{q=0} \tag{30}$$

The convergence of above series depends upon the values of $\hbar_f$, $\hbar_\theta$ and $\hbar_\phi$. We consider that $\hbar_f$, $\hbar_\theta$ and $\hbar_\phi$ are selected properly such that Eqs. (27)−(29) converge at q=1 then we have

$$f(\eta) = f_0(\eta) + \sum_{m=1}^{\infty} f_m(\eta) \tag{31}$$

$$\theta(\eta) = \theta_0(\eta) + \sum_{m=1}^{\infty} \theta_m(\eta) \tag{32}$$

$$\phi(\eta) = \phi_0(\eta) + \sum_{m=1}^{\infty} \phi_m(\eta) \tag{33}$$

The general solutions can be written as

$$f_m(\eta) = f_m^*(\eta) + C_1 + C_2 e^{\eta} + C_3 e^{-\eta} \tag{34}$$

$$\theta_m(\eta) = \theta_m^*(\eta) + C_4 e^{\eta} + C_5 e^{-\eta} \tag{35}$$

$$\phi_m(\eta) = \phi_m^*(\eta) + C_6 e^{\eta} + C_7 e^{-\eta} \tag{36}$$

where f_m^*, θ_m^* and $\phi_m^*(\eta)$ are the special solutions.

4 Convergence of homtopy solutions and discussion

Obviously, the homotopy solutions contain the auxiliary parameters $\hbar_f$, $\hbar_\theta$ and $\hbar_\phi$ which are responsible for adjusting and controlling the convergence of the derived solutions. To find the suitable values of these auxiliary parameters, we plot the $\hbar$-curves at 26th-order of HAM approximations. Figure 1 indicates that the suitable values of $\hbar_f$, $\hbar_\theta$ and $\hbar_\phi$ are $-0.98 \le \hbar_f \le -0.10, -1.0 \le \hbar_\theta \le -0.30, -1.0 \le \hbar_\phi \le -0.3$. The series converges in the whole region of η when $\hbar_f = -0.6$ and $\hbar_\theta = \hbar_\phi = -0.7$ (see Table 1).

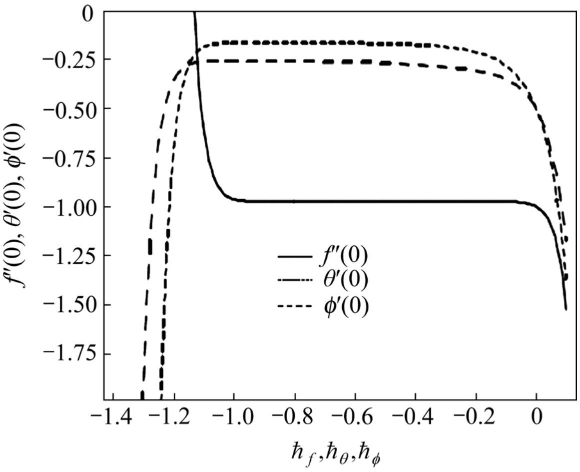

Fig. 1 $\hbar$-curves for functions $f(\eta)$, $\theta(\eta)$ and $\phi(\eta)$ at 20th-order of approximations when β=1.2, M=0.6, Pr=1.0, Le=0.7, N_t=0.4=N_b, Bi_1=0.7=Bi_2 and Ec=0.8

Table 1 Convergence of homotopy solution for different order of approximations when β=1.0, M=0.5, Pr=0.7, Le=0.5, N_t=0.2, N_b=0.7, Bi_1=1.0=Bi_2, Ec=0.3, $\hbar_f = -0.6$ and $\hbar_\theta = \hbar_\phi = -0.7$

Order of approximation	$-f''(0)$	$-\theta'(0)$	$-\phi'(0)$
1	0.975000	0.36554	0.40208
10	0.974040	0.17855	0.28087
15	0.974039	0.17078	0.26913
30	0.974039	0.16758	0.25763
40	0.974039	0.16749	0.25576
50	0.974039	0.16749	0.25509
55	0.974039	0.16749	0.25509
60	0.974039	0.16749	0.25509

We analyze the variations of Casson parameter β, magnetic parameter M, Prandtl number Pr, Lewis number Le, Biot number Bi_1, thermophoretic parameter N_t, Brownian motion parameter N_b and Eckert number Ec on the dimensionless temperature $\theta(\eta)$ (see Figs. 2−9). Figure 2 witnesses that the temperature and thermal boundary layer thickness decrease for the higher values of Casson parameter. Higher value of Casson parameter corresponds to a decrease in the yield stress that causes a reduction in the fluid temperature and thermal boundary layer thickness. Figure 3 illustrates the effects of magnetic parameter on the temperature. Here, an increase in magnetic parameter leads to an enhancement in the temperature. Physically, larger value of magnetic parameter shows stronger Lorentz force. Such stronger Lorentz force is an agent providing more heat to fluid due to the fact that higher temperature and thicker thermal boundary layer thickness occur. Figure 4 shows that the temperature and thermal boundary layer thickness decrease for higher Prandtl numbers. Prandtl number is the ratio of momentum diffusivity to thermal diffusivity. For higher Prandtl fluids the

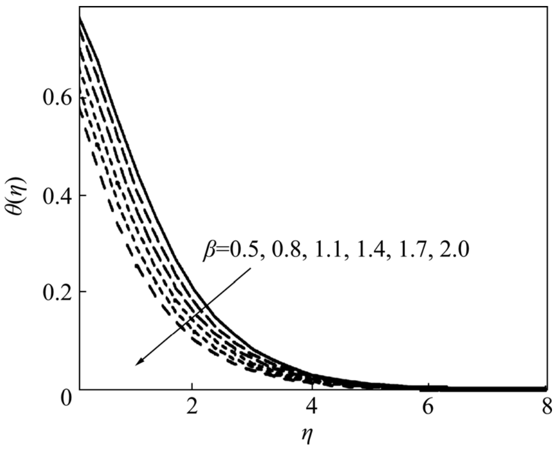

Fig. 2 Temperature distribution function $\theta(\eta)$ vs η corresponding to different values of β when M=0.6=Le, Pr=0.8, Bi_1=1.0=Bi_2, N_t=0.4=N_b and Ec=0.5

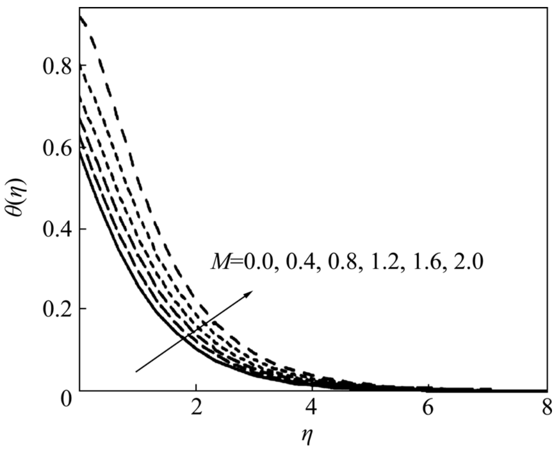

Fig. 3 Temperature distribution function $\theta(\eta)$ vs η corresponding to different values of M when β=1.2, Pr=0.8, Le=0.6, Bi_1=1.0=Bi_2, N_t=0.4=N_b and Ec=0.5

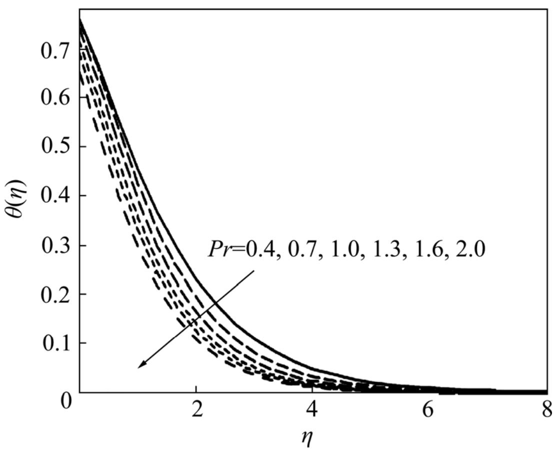

Fig. 4 Temperature distribution function $\theta(\eta)$ vs η corresponding to different values of Pr when β=1.2, M=0.6=Le, Bi_1=1.0=Bi_2, N_t=0.4=N_b and Ec=0.5

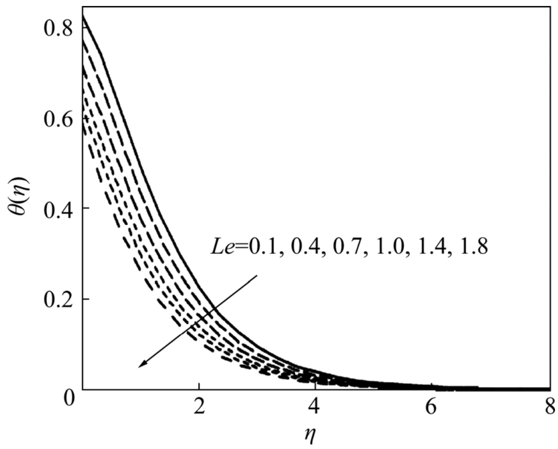

Fig. 5 Temperature distribution function $\theta(\eta)$ vs η corresponding to different values of Le when β=1.2, M=0.6, Pr=0.8, Bi_1=1.0=Bi_2, N_t=0.4=N_b and Ec=0.5

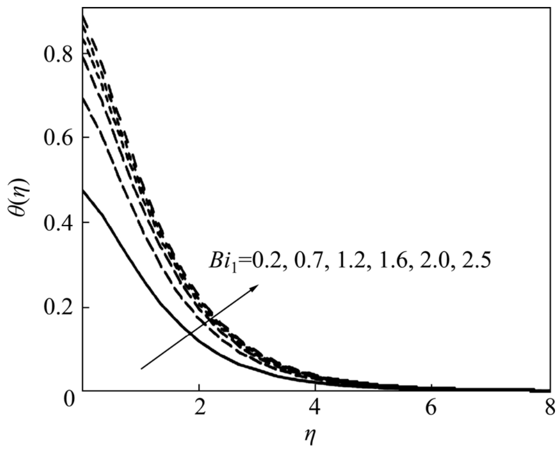

Fig. 6 Temperature distribution function $\theta(\eta)$ vs η corresponding to different values of Bi_1 when β=1.2, M=0.6=Le, Pr=0.8, Bi_2=1.0, N_t=0.4=N_b and Ec=0.5

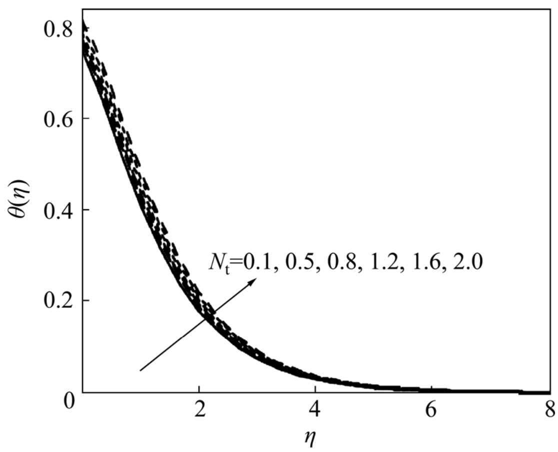

Fig. 7 Temperature distribution function $\theta(\eta)$ vs η corresponding to different values of N_t when β=1.2, M=0.6=Le, Pr=0.8, Bi_1=1.0=Bi_2, N_b=0.4 and Ec=0.5

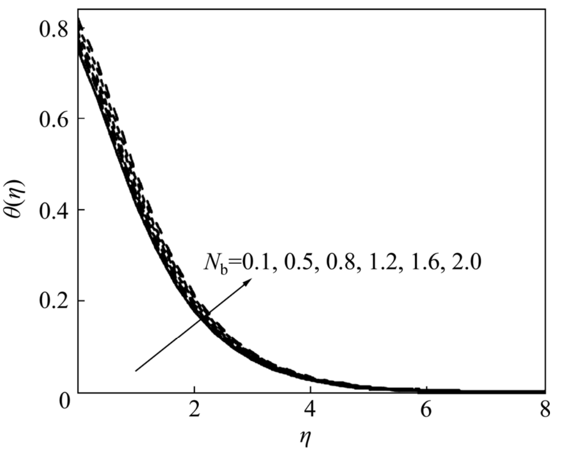

Fig. 8 Temperature distribution function $\theta(\eta)$ vs η corresponding to different values of N_b when β=1.2, M=0.6=Le, Pr=0.8, Bi_1=1.0=Bi_2, N_t=0.4 and Ec=0.5

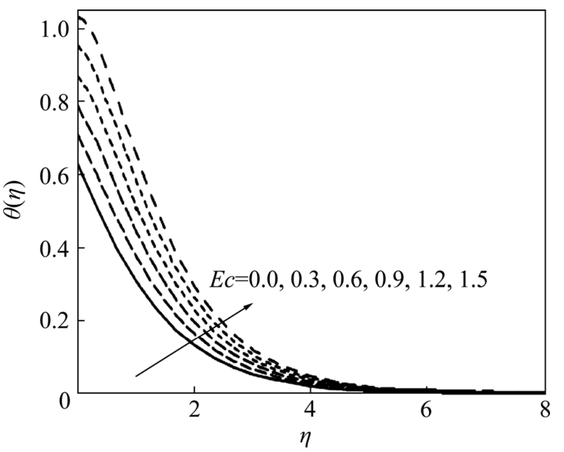

Fig. 9 Temperature distribution function $\theta(\eta)$ vs η corresponding to different values of Ec when β=1.2, M=0.6=Le, Pr=0.8, Bi_1=1.0=Bi_2 and N_t=0.4=N_b

momentum diffusivity increases while there is decrease in the thermal diffusivity. Here, a decrease in thermal diffusivity dominant is over an increase in the momentum diffusivity. This change in thermal diffusivity shows lower temperature and thinner thermal boundary layer. The variations in temperature profile for various values of Lewis number are seen in Fig. 5. Temperature increases for smaller values of Lewis number while it increases for higher values of Le. It is known that higher Lewis number fluid has smaller Brownian diffusion coefficient and lower Lewis number fluid has higher Brownian diffusion coefficient. This produces a change in temperature and thermal boundary layer thickness. Figure 6 depicts the change in temperature profile for different values of Biot number Bi_1. Temperature increases rapidly for Bi_1=0.2, 0.7 but the change in temperature for Bi_1=1.2 and so on is very small. Here, we conclude that the change in temperature for smaller values of Bi_1 is higher while such change is smaller for larger values of Bi_1. Figures 7 and 8 elucidate that both temperature and thermal boundary layer thickness increase through larger thermophoretic and Brownian motion parameters. Figure 9 analyzes that temperature is larger for higher values of Eckert number.

Figures 10−16 are drawn to examine the change in nanoparticle concentration distribution $\phi(\eta)$ for different values of Casson parameter β, magnetic parameter M, Prandtl number Pr, Lewis number Le, Biot number Bi_2, hermophoretic parameter N_t and Brownian motion parameter N_b. Figures 10 and 11 clearly show that Casson and magnetic parameters have similar effects on the nanoparticle concentration and temperature fields. Figures 12 and 13 indicate that the nanoparticle concentration and its related boundary layer thickness decreases when we increase the values of Prandtl and Lewis numbers. An increase in Biot number Bi_2 gives rise to the nanoparticle concentration profile. Nanoparticle concentration profile increases rapidly for Bi_2=0.2, 0.7 but this change in nanoparticle concentration is slow down when Bi_2=1.2 and so on (see Fig. 14). In fact, Bi_2 involves the Brownian diffusion coefficient.

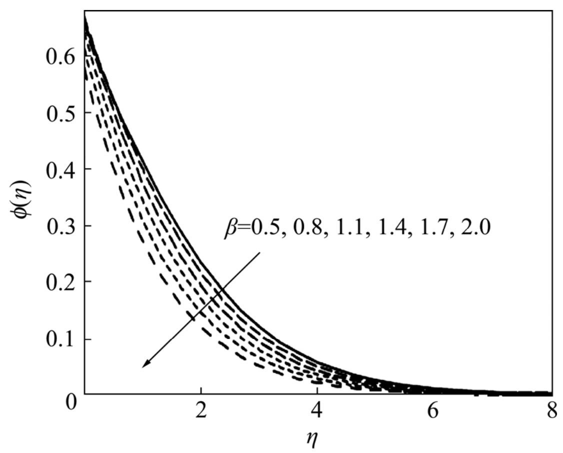

Fig. 10 Nanoparticle concentration distribution function $\phi(\eta)$ vs η corresponding to different values of β when M=0.6=Le, Pr=0.8, Bi_1=1.0=Bi_2, N_t=0.4=N_b and Ec=0.5

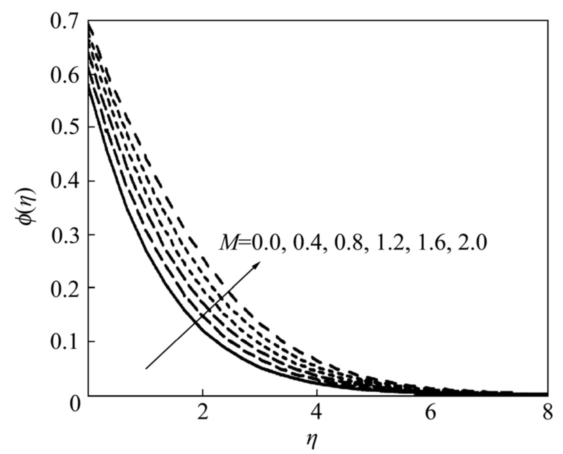

Fig. 11 Nanoparticle concentration distribution function $\phi(\eta)$ vs η corresponding to different values of M when β=1.2, Le=0.6, Pr=0.8, Bi_1=1.0=Bi_2, N_t=0.4=N_b and Ec=0.5

Brownian diffusion coefficient increases when we increase the values of Bi_2. This increase in Brownian diffusion coefficient leads to the higher nanoparticle concentration. Figures 15 and 16 show that the nanoparticle concentration is an increasing function of thermophoretic parameter while on the other hand we observed that the nanoparticle concentration decreases when Brownian motion parameter increases. Figure 16 illustrates that the change in nanoparticle concentration corresponding to N_b=0.1, 0.5 is more dominant as we observed for N_b=0.8 and so on. Table 1 provides the convergence values of $-f''(0)$, $-\theta'(0)$ and $-\phi'(0)$ when β=1.0, M=0.5=Le, Pr=0.7, N_t=0.2, N_b=0.7, Bi_1=1.0=Bi_2, Ec=0.3, $\hbar_f=-0.6$ and $\hbar_\theta=-0.7=\hbar_\phi$. Here, we have seen that the solution of $-f''(0)$ converge from 15th-order of deformations while the solutions of $-\theta'(0)$ and $-\phi'(0)$ converge form 40th- and 50th-order of approximations, respectively. Table 2 presents the numerical values of skin-friction coefficient $(1+1/\beta)f''(0)$ for various values of β and M. The values of skin-friction coefficient are decreased by increasing β but it increases for higher values of magnetic parameter M. Table 3 shows an excellent agreement with the previous numerical and homotopic solutions in a limiting case.

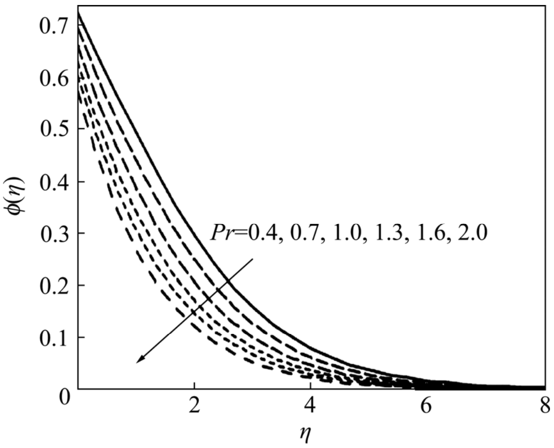

Fig. 12 Nanoparticle concentration distribution function $\phi(\eta)$ vs η corresponding to different values of Pr when β=1.2, M=0.6=Le, Bi_1=1.0=Bi_2, N_t=0.4=N_b and Ec=0.5

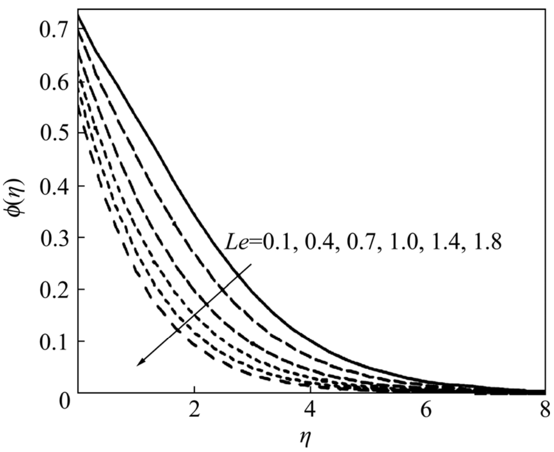

Fig. 13 Nanoparticle concentration distribution function $\phi(\eta)$ vs η corresponding to different values of Le when β=1.2, M=0.6, Pr=0.8, Bi_1=1.0=Bi_2, N_t=0.4=N_b and Ec=0.5

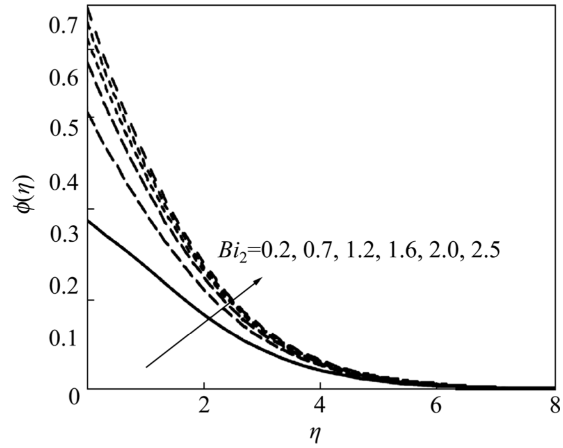

Fig. 14 Nanoparticle concentration distribution function $\phi(\eta)$ vs η corresponding to different values of Bi_2 when β=1.2, M=0.6=Le, Pr=0.8, Bi_1=1.0, N_t=0.4=N_b and Ec=0.5

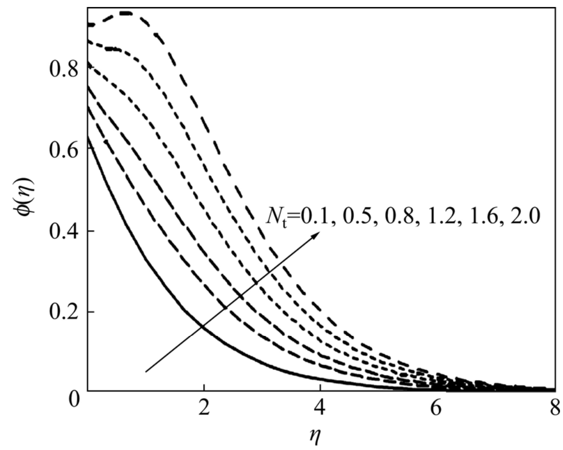

Fig. 15 Nanoparticle concentration distribution function $\phi(\eta)$ vs η corresponding to different values of N_t when β=1.2, M=0.6=Le, Pr=0.8, Bi_1=1.0=Bi_2, N_b=0.4 and Ec=0.5

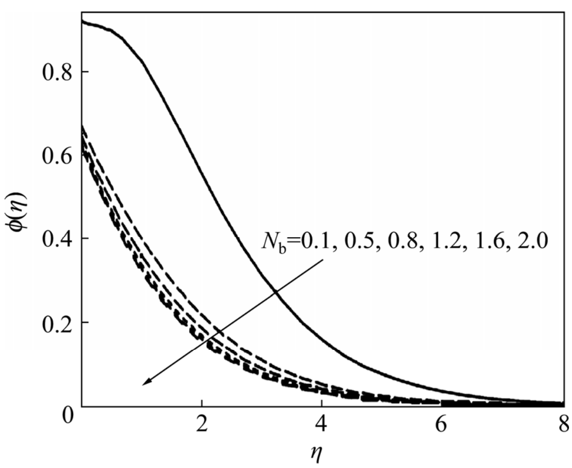

Fig. 16 Nanoparticle concentration distribution function $\phi(\eta)$ vs η corresponding to different values of N_b when β=1.2, M=0.6=Le, Pr=0.8, Bi_1=1.0=Bi_2, N_t=0.4 and Ec=0.5

Table 2 Numerical values of skin-friction coefficient $(1+1/\beta)f''(0)$ for different values of β and M

β	M	$-(1+1/\beta)f''(0)$
0.7	0.5	2.146677
1.2		1.865142
1.6		1.755974
2.0		1.687085
1.2	0.0	1.735577
	0.4	1.819679
	0.7	1.980908
	1.2	2.205917

Table 3 Comparison of values of $-\theta'(0)$ for different values of Pr with previous existing results when $N_t=N_b=0.0$, $\beta\to\infty$ and $Bi_1=1000$

Pr	$-\theta'(0)$		
	Present result	Ref. [21]	Ref. [22]
0.07	0.06637	0.0663	0.0663
0.20	0.61913	0.1691	0.1691
0.70	0.45395	0.4539	0.4539
2.00	0.91132	0.9113	0.9113

5 Conclusions

1) Higher value of Casson parameter leads to a decrease in the temperature and nanoparticle concentration.

2) Effects of Lewis number on nanoparticle concentration are more pronounced in comparison with the temperature.

3) Increasing values of Biot numbers Bi_1 and Bi_2 correspond to an increase in the fluid temperature and nanoparticle concentration.

4) Temperature is enhanced for the higher values of thermophoresis and Brownian motion parameters.

5) Effects of thermophoresis and Brownian motion parameters on nanoparticle concentration are quite opposite.

References

[1] SHARMA A, TYAGI V V, CHEN C R, BUDDHI D. Review on thermal energy storage with phase change materials and applications [J]. Renewable and Sustainable Energy Review, 2009, 13: 318 −345.

[2] CHOI S U S, EASTMAN J A. Enhancing thermal conductivity of fluids with nanoparticles [C]// ASME Internatimal Mechanical Engineering Congress & Exposition. San Francisco, 1995, 66: 99−105.

[3] HOSSEINI M, GHADER S. A model for temperature and particle volume fraction effect on nanofluid viscosity [J]. Journal of Molecular Liquids, 2010, 153: 139−145.

[4] KANDASAMY R, LONGATHAN P, ARASU P P. Scaling group transformation for MHD boundary-layer flow of a nanofluid past a vertical stretching surface in the presence of suction/injection [J]. Nuclear Engineering and Design, 2011, 241: 2053−2059.

[5] KAMESWARAN P K, NARAYANA M, SIBANDA P, MURTHY P V S N. Hydromagnetic nanofluid flow due to a stretching or shrinking sheet with viscous dissipation and chemical reaction effects [J]. International Journal of Heat and Mass Transfer, 2012, 55: 7587−7595.

[6] TURKYILMAZOGLU M. Exact analytical solutions for heat and mass transfer of MHD slip flow in nanofluids [J]. Chemical Engineering Science, 2012, 84: 182−187.

[7] RASHIDI M M, ABELMAN S, MEHR N F. Entropy generation in steady MHD flow due to a rotating porous disk in a nanofluid [J]. International Journal of Heat and Mass Transfer, 2013, 62: 515−525.

[8] HATAMI M, NOURI R, GANJI D D. Forced convection analysis for MHD Al_2O_3−water nanofluid flow over a horizontal plate [J]. Journal of Molecular Liquids, 2013, 187: 294−301.

[9] MAKINDE O D, KHAN W A, KHAN Z H. Buoyancy effects on MHD stagnation point flow and heat transfer of a nanofluid past a convectively heated stretching/shrinking sheet [J]. International Journal of Heat and Mass Transfer, 2013, 62: 526−533.

[10] HATAMI M, GANNJI D D. Heat transfer and flow analysis for SA-TiO_2 non-Newtonian nanofluid passing through the porous media between two coaxial cylinders [J]. Journal of Molecular Liquids, 2013, 188: 155−161.

[11] MOTSA S S, SHATEYI S, MUKUKULA Z. Homotopy analysis of free convection boundary layer flow with heat and mass transfer [J]. Chemical Engineering Communications, 2011, 198: 783−795.

[12] MAHMOOD M, ASGHAR S, HOSSAIN M A. Transient mixed convection flow arising due to thermal and mass diffusion over porous sensor surface inside squeezing horizontal channel [J]. Applied Mathematics and Mechanics: English Edition, 2013, 34: 97−112.

[13] TURKYILMAZOGLU M. Heat and mass transfer of MHD second order slip flow [J]. Computers & Fluids, 2013, 71: 426−434.

[14] ALSAADI F E, SHEHZAD S A, HAYAT T, MONAQUEL S J. Soret and Dufour effects on the unsteady mixed convection flow over a stretching surface [J]. Journal of Mechanics, 2013, 29: 623−632.

[15] FERDOWS M, UDDIN Md J, AFIFY A A. Scaling group transformation for MHD boundary layer free convective heat and mass transfer flow past a convectively heated nonlinear radiating stretching sheet [J]. International Journal of Heat and Mass Transfer, 2013, 56: 181−187.

[16] AZIZ A. A similarity solution for laminar thermal boundary layer over a flat plate with a convective surface boundary condition [J]. Communications in Nonlinear Sciences and Numerical Simulation, 2009, 14: 1064−1068.

[17] MAKINDE O D, AZIZ A. MHD mixed convection from a vertical plate embedded in a porous medium with a convective boundary condition [J]. International Journal of Thermal Sciences, 2010, 49: 1813−1820.

[18] HAMAD M A A, UDDIN Md J, ISMAIL A I Md. Investigation of combined heat and mass transfer by Lie group analysis with variable diffusivity taking into account hydrodynamic slip and thermal convective boundary conditions [J]. International Journal of Heat and Mass Transfer, 2012, 55: 1355−1362.

[19] SHEHZAD S A, ALSAEDI A, HAYAT T. Three-dimensional flow of Jeffery fluid with convective surface boundary conditions [J]. International Journal of Heat and Mass Transfer, 2012, 55: 3971−3976.

[20] HAYAT T, WAQAS M, SHEHZAD S A, ALSAEDI A. Mixed convection radiative flow of Maxwell fluid near a stagnation point with convective condition [J]. Journal of Mechanics, 2013, 29: 403−409.

[21] MAKINDE O D, AZIZ A. Boundary layer flow of nanofluid past a

stretching sheet with a convective boundary condition [J]. International Journal of Thermal Sciences, 2011, 50: 1326−1332.
[22] ALSAEDI A, AWAIS M, HAYAT T. Effects of heat generation/absorption on stagnation point flow of nanofluid over a surface with convective boundary conditions [J]. Communications in Nonlinear Sciences and Numerical Simulation, 2012, 17: 4210−4223.
[23] SHAHMOHAMADI H. Analytic study on non-Newtonian natural convection boundary layer flow with variable wall temperature on a horizontal plate [J]. Meccanica, 2012, 47: 1313−1323.
[24] HAYAT T, SHEHZAD S A, ALSAEDI A. Soret and Dufour effects on magnetohydrodynamic (MHD) flow of Casson fluid [J]. Applied Mathematics and Mechanics: English Edition, 2012, 33: 1301−1312.
[25] MUKHOPADHYAY S, VAJRAVELU K, van GORDER R A. Casson fluid flow and heat transfer at an exponentially stretching permeable surface [J]. Journal of Applied Mechanics, 2013, 80: 054502.
[26] LIAO S J. Homotopy analysis method in nonlinear differential equations [M]. Heidelberg: Springer & Higher Education Press, 2012.
[27] TURKYILMAZOGLU M. Solution of the Thomas−Fermi equation with a convergent approach [J]. Communications in Nonlinear Sciences and Numerical Simulation, 2012, 17: 4097−4103.
[28] ABBASBANDY S, HASHEMI MS, HASHIM I. On convergence of homotopy analysis method and its application to fractional integro-differential equations [J]. Quaestiones Mathematicae, 2013, 36: 93−105.
[29] HASSAN N, RASHIDI M M. An analytic solution of micro polar flow in a porous channel with mass injection using homotopy analysis method [J]. International Journal of Numerical Methods for Heat & Fluid Flow, 2014, 24: 419−437.
[30] SHEHZAD S A, HAYAT T, ALHUTHALI M S, ASGHAR S. MHD three-dimensional flow of Jeffrey fluid with Newtonian heating [J]. Journal of Central South University, 2014, 21: 1428−1433.

(Edited by YANG Hua)